Clim. Past Discuss., 5, 1133–1162, 2009
www.clim-past-discuss.net/5/1133/2009/

Climate of the Past Discussions

Climate of the Past Discussions is the access reviewed discussion forum of *Climate of the Past*

Sources of holocene variability of oxygen isotopes in paleoclimate archives

A. N. LeGrande and G. A. Schmidt

NASA Goddard Institute for Space Studies and Center for Climate Systems Research, Columbia University, 2880 Broadway, New York, NY 10025, USA

Received: 6 March 2009 – Accepted: 10 March 2009 – Published: 23 March 2009

Correspondence to: A. N. LeGrande (legrande@giss.nasa.gov)

Published by Copernicus Publications on behalf of the European Geosciences Union.

Abstract

Variability in water isotopes has been captured in numerous archives and used to infer climate change. Here we examine water isotope variability over the course of the Holocene using the water-isotope enabled, coupled atmosphere-ocean general circulation model, GISS ModelE-R. Eight Holocene time slices, mostly 1000 years apart are simulated using estimated changes in orbital configuration, greenhouse gases, and ice sheet extent. We find that water isotopes in the model match well with those captured in proxy climate archives in ice cores, ocean sediment cores, and speleothems. The climate changes associated with the water isotope changes, however, are more complex than simple modern analog interpretations. In particular, water isotope variability in Asian speleothems is linked to alterations in landward water vapor transport, not local precipitation, and ice sheet changes over North America lead to masking of temperature signals in Summit, Greenland. Salinity-seawater isotope variability is complicated by inter-ocean basin exchanges of water vapor. Water isotopes do reflect variability in the hydrologic cycle, but are better interpreted in terms of regional changes rather than local climate variables.

1 Introduction

Water isotopes are important tracers of the hydrologic cycle. In the atmosphere, the oxygen isotopic composition of precipitation, $\delta^{18}O_{prec}$ (δ refers to the ratio of the sample concentration to a known standard) is a product of the initial composition of $\delta^{18}O$ in the water vapor of an air parcel and the amount of rain out and mixing of that air parcel along its path. It is correlated to surface air temperature at mid to high latitudes and thought to correlate to the amount of precipitation at low latitudes over short time periods (Dansgaard, 1964). Long term records of $\delta^{18}O_{prec}$ available in ice cores, speleothems, lake records, and tree cellulose provide a way to infer information about climate if appropriate interpretations can be found (Cuffey et al., 1995; Jouzel et al.,

CPD

5, 1133–1162, 2009

2003; Roden et al., 2000; Wang et al., 2001).

Similarly, the oxygen isotopic composition of seawater, $\delta^{18}O_{sw}$ is a tracer of circulation and of surface ocean fluxes. In the ocean, $\delta^{18}O_{sw}$ is regionally related to salinity since fluxes of freshwater (precipitation and evaporation) affect the concentration of both. Variations in $\delta^{18}O_{sw}$ are more complicated than salinity since water isotopes undergo additional fractionation and transport in the atmosphere (Craig and Gordon, 1965).

The concentration of $\delta^{18}O_{sw}$ is preserved in the calcite shells of marine microfossils such as foraminifera as well as the aragonite skeletons of corals. These ratios are complicated by a temperature dependent fractionation of −1‰ per 5°C of $\delta^{18}O$ (Epstein et al., 1953) and species dependent "vital effects". Past variability in $\delta^{18}O_{sw}$ can potentially be reconstructed given paired measurements of $\delta^{18}O$ in calcite and an independent temperature proxy (e.g., Mg/Ca in calcite), giving insight into the past hydrologic cycle (Schmidt et al., 2004).

Alterations in orbital configuration have long been postured as the primary driver of climate change over the last 10 000 years. Holocene perihelion changes enhanced Northern Hemisphere seasonality, with the maximum changes occurring in the early Holocene. In the tropics, the monsoon was likely more intense in the early Holocene, with intensity diminishing through the modern (Maher, 2008).

The key to interpreting the signals in paleoclimate records is an estimate of the temporal gradient. Often people have applied modern spatial gradients, but these need not be the same as temporal gradients. Further, temporal gradients of different lengths may also be variable.

In the ocean, variability in $\delta^{18}O_{sw}$ has been used to infer past salinity variability given the modern (regional) relationship between $\delta^{18}O_{sw}$ and salinity (Schmidt et al., 2004; Stott et al., 2004). These reconstructions assume that the modern regional (spatial) relationship – which is the regression of the $\delta^{18}O_{sw}$ to salinity relationship over a region – was valid over a range of timescales at a finite point in space; i.e., the reconstructions of salinity assume that the temporal relationship between the two

CPD
5, 1133–1162, 2009

is equivalent to the spatial relationship. Since the hydrologic cycle itself – including atmospheric variations in $\delta^{18}O$ – is impacted by climate, this assumption has been called into question (Schmidt, 1999). During times of climate change, it is possible that the relationship of $\delta^{18}O_{sw}$ to salinity and $\delta^{18}O_{prec}$ to precipitation/temperature have also changed.

Are the spatial relationships derived from the modern distribution of water isotopes and climate equivalent to temporal relationships? In Greenland, paired measurements of water isotopes and borehole temperatures establish that the spatial ratio between temperature and $\delta^{18}O_{prec}$ regionally are roughly twice the temporal ratio between the two (Cuffey et al., 1995; Werner et al., 2000). Ice records from Antarctica at present do not seem to have the same complicating factor (Jouzel et al., 2003). However, the potential for such divergence in temporal and spatial ratios suggests that further, site and proxy-specific work is required.

Future climate, given a business as usual scenario, will likely be significantly warmer than today. However, climate models have been thoroughly tested on the range of climate variability over the last 100 years. Future climate, given a business as usual scenario, will likely extend beyond this range. Therefore models need to be tested over a greater range of variability as is inferred from the paleoclimate record. Since early to mid-Holocene Northern Hemisphere Holocene climate was likely different than today, it is a good target to test climate model performance outside the modern range. Because of this benefit as well as well known boundary conditions, mid-Holocene (6000 BP) climate changes are regularly simulated as part of model-data inter-comparison projects that attempt to quantify the skill of climate models outside the modern range (e.g., PMIP2: Masson-Delmotte et al., 2006). These comparisons are useful in highlighting model skills and deficits. Several questions remain: how will changes in surface air temperature gradients and Hadley circulation impact the inter-tropical convergence zone? How would meridional overturning circulation be impacted by melting of ice sheets, particularly in the Early Holocene, during the last phases of the deglaciation?

Here we explore the variability of the $\delta^{18}O$ over the Holocene (last 10 000 years)

CPD
5, 1133–1162, 2009

using a fully coupled atmosphere-ocean general circulation model (GCM) that explicitly tracks water isotopes throughout the hydrologic cycle. We quantify the impact of orbital variations, (small) greenhouse gas variations, and ice sheet variation in order to (1) examine the amount of variability of the proxy records compared to climate, (2) assess the skill of the model in reproducing the Holocene climate variability, and (3) suggest improvements to the interpretation of isotopic data from this period.

2 Methods and model description

GISS ModelE-R (Goddard Institute for Space Studies ModelE-R) is a fully coupled atmosphere/ocean GCM. The experiments here use the M20 version of ModelE whose horizontal resolution is 4°×5°, with a 20 vertical layer atmosphere up to 0.1 hPa height (Schmidt et al., 2006) coupled to the 13-layer Russell Ocean model at the same horizontal resolution (Hansen et al., 2007). Atmospheric advection uses the quadratic upstream scheme, with 9 moments advected in addition to mean quantities, significantly enhancing the effective tracer resolution (to ~1.3°×~1.6°). The ocean model is non-Boussinesq, mass conserving, and has a full free surface. Freshwater is treated in a "natural" way; i.e., the addition of freshwater increases the free surface and reduces salinity purely through dilution. No equivalent salt fluxes or flux adjustments are used, allowing for the prognostic calculation of water isotope to salinity relationships. All boundary conditions and atmospheric composition in the control case are appropriate to the pre-industrial period (circa 1880).

Water tracers ($^{1}H_2^{16}O$, "normal" water; $^{2}H^{1}H^{16}O$, δD; $^{1}H_2^{18}O$, $\delta^{18}O$; where δ in permil (‰) $\equiv [(R_{std}/R_{smow})-1]$ X 1000) are included in the atmosphere, land surface, sea ice, and ocean and are tracked through all stages of the hydrologic cycle (Schmidt et al., 2007). These isotopes are advected like water through the model, but at each phase change, an appropriate fractionation is performed (Schmidt et al., 2005).

Eight "time slice" experiments were performed, giving roughly 1000 year temporal coverage across the Holocene (Table 1). In each, greenhouse gas concentrations

CPD
5, 1133–1162, 2009

were adjusted based on ice core reconstructions (Brook et al., 2000; Indermuhle et al., 1999; Sowers et al., 2003), and seasonal insolation was changed as a function of changing orbital parameters (Berger and Loutre, 1991). For the 9 kya (kilo-years ago) experiment, a remnant Laurentide ice sheet was included (Licciardi et al., 1998, Fig. 1), and mean ocean water salinity and $\delta^{18}O$ adjusted to account for ice volume (equivalent to ~35 m of sea level) changes (Fairbanks, 1989). Each experiment was run 500 years, reaching quasi-equilibrium, and the last 100 years of the experiments are presented here.

3 Results

To facilitate comparisons, changes are reported in past anomalies compared to present (0 k, pre-Industrial) simulations. Thus, statements about cooler temperatures or less rainfall refer to cooler temperatures or less rainfall in the past relative to the 0 kyr simulation.

3.1 Large scale climate changes

Northern Hemisphere extra-tropical insolation was significantly enhanced in summer, and somewhat reduced in winter; in the early Holocene (EH≡9 kya simulation) boreal summers received up to 60 W/m^2 greater insolation, while boreal winter insolation was somewhat reduced (~15 W/m^2). Compared to the pre-industrial, Holocene greenhouse gas forcing was reduced, yielding a radiative forcing of ~−0.7 W/m^2 in the EH to mid-Holocene (MH≡6 kya simulation). Cumulatively, these forcings caused annual mean warming in the Northern Hemisphere, up to 2–3°C, with cooling the Southern Hemisphere around 1°C (annual average, Fig. 2) in the mid-Holocene. In general, anomalies have similar patterns, but greater magnitudes in the early Holocene compared to the MH compared to the Late Holocene (LH≡3 kya simulation).

Simulated summer sea ice decreases by ~5% in the Arctic in the early Holocene;

though changes in sea ice may be underestimated in ModelE-R since the sea ice in this version of the model is relatively (and possibly erroneously) insensitive to warming Arctic temperatures (Stroeve et al., 2007). Early Holocene boreal summer temperature anomalies reach 4°C in interior regions of Eurasia as well as the Canadian Arctic (Fig. 3). Greenland Surface Air Temperatures (SATs) are simulated to be 1–2°C warmer in summer. Boreal winter SATs are largely cooler over land, but warmer over the Arctic Ocean resulting from a persistent reduction in sea ice, with anomalies approximately half the magnitude of those in summer. Boreal summer land-sea SAT contrast is enhanced in all Holocene simulations compared to the modern, with the greatest contrast in the Early to Mid-Holocene simulations. These changes are consistent with climate reconstructions of North America and Europe showing maximum summer warmth attained 7000–9000 years ago, and decreasing temperatures into the pre-Industrial (Wanner et al., 2008).

In the early Holocene, the (remnant) Laurentide ice sheet (LIS – inferred to be 3000 m thick in places, though isostatic compensation makes the surface height anomaly relative to modern smaller by ~2/3 (Licciardi et al., 1998)) yields local cooling of up to 12°C. Additionally, the orographic forcing of the remnant ice sheet itself causes a southward deflection of the atmospheric jets, yielding further cooling downstream over Greenland and eastward into the western GIN (Greenland/Iceland/Norwegian) Seas (Carlson et al., 2008).

Surface solar forcing of ~20 W/m^2 (greater than today) over the remnant Laurentide ice sheet (LIS) induces melting of the LIS in our simulation, which leads to a fresher Labrador Sea (Carlson et al., 2008). LIS glacial melt water is specified to be fresh with $\delta^{18}O_{ice}$ the average of $\delta^{18}O_{prec}$ over Northern Hemisphere land ice. LIS melt enters the ocean as "ice bergs" in the upper 200 m of the water column, causing alterations to the upper ocean density structure of the Labrador Sea, suppressing the formation of deep water. This leads to a reduction in the early Holocene simulated North Atlantic Deep Water (NADW: 48° N, 900 m) of ~23% due to the lack of deep seawater formation in the Labrador Sea.

CPD
5, 1133–1162, 2009

In all other simulations, simulated NADW is steady (~22±1 Sv), consistent with proxy indicators (McManus et al., 2004). This transition in NADW production as the LIS disappears is similar to proxy records that indicate deep water production in the Labrador Sea was absent until around 7000 BP (Hillaire-Marcel et al., 2001). The inferred change at that time is postulated to have been due to the deglaciation that was still ongoing through around 6500 BP, when eustatic sea level reached near-modern levels (Carlson et al., 2007). In the Early Holocene, the lack of Labrador Deep Sea Water production temperatures yields regionally cooler SAT by 1–2°C. There is also a reduction in precipitation over the Labrador Sea convection areas.

Sea surface temperatures (SST) in the Northern Hemisphere are warmer in the earlier periods. Generally, this pattern is greatest in the Early Holocene, with decreases in insolation and Northern Hemisphere temperature into the modern. Lower greenhouse gases yield slight SST cooling in the tropics and Southern Hemisphere. As a result, SST gradients are altered, and the simulated ITCZ (Inter-tropical Convergence Zone) shifts northward (Figs. 2 and 3) in the Holocene, consistent with proxy estimates (Haug et al., 2001; Pearman et al., 2008).

This alteration has important consequences for inter-ocean basin salinity gradients. In particular, water vapor transport across the Isthmus of Panama, a phenomenon important in maintaining the modern Atlantic to Pacific 1 psu salinity gradient, reduces by ~5% in the Mid-Holocene (Fig. 4). This alteration leads to a decrease in the Atlantic to Pacific salinity contrast in the Holocene simulations.

Latent heat and cloudiness changes associated with the simulated ITCZ movement yield cooling over West Africa and eastward into the Middle East. Precipitation changes over Asia are generally small with both positive and negative anomalies, with the saddle centered over the Himalayas. Precipitation over the Western Tropical Pacific warm pool, the Western Atlantic into the Caribbean, and south-east Asia is reduced, particularly in boreal winter. Boreal summer precipitation increases broadly over West Africa eastward into India (Fig. 3).

3.2 Isotopic changes

Warmer temperatures and reductions in Arctic sea ice across the Arctic and the Northern Hemisphere are generally associated with heavier $\delta^{18}O_{prec}$ in 6 kya through 1 kya simulations relative to modern (Fig. 2). Isotopic anomalies in the early Holocene, however, are more complex and complicated by the impacts of the remnant ice. The negative mass balance of the LIS reduces NADW which yields cooler temperatures associated with lighter $\delta^{18}O_{prec}$. In addition, the melt water is highly depleted in $\delta^{18}O$ reinforcing lighter regional $\delta^{18}O_{prec}$ values near the LIS. These competing effects in the early Holocene yield a front between negative and positive $\delta^{18}O_{prec}$ anomalies (Fig. 3). The simulation of this front will likely not precisely replicate that realized in the early Holocene; however, the simulation is instructive since it suggests that such a pattern may have existed in the past.

Topographic changes further complicate Greenland $\delta^{18}O_{prec}$ changes in the early Holocene. The existence of the LIS forces atmospheric jets to divert southward (Carlson et al., 2008). In the absence of North American ice sheets, water vapor from Pacific supplies a significant proportion of boreal summer moisture to Summit (~30% in this version of ModelE-R). In the early Holocene, there is a relatively greater amount of rainfall with more local sources, such as the Labrador and Greenland Seas. These shorter pathways results in an air mass that retains a greater amount of heavier isotope in the water vapor once it reaches Greenland. Heavier $\delta^{18}O_{prec}$ values can thus occur even if temperatures were held constant. In the simulated early Holocene, Summit temperatures are cooler, but no significant $\delta^{18}O_{prec}$ changes are observed, largely as a result of the shorter pathway for water vapor from the ocean to Summit. This complexity in the Greenland $\delta^{18}O_{prec}$ signal may induce large magnitude changes in Greenland ice core $\delta^{18}O_{prec}$ records (Charles et al., 1995).

The simulated front between positive and negative anomalies in temperature is slightly different to that in $\delta^{18}O_{prec}$ because of these orographic changes. Where this mismatch occurs, standard high latitude temperature to $\delta^{18}O_{prec}$ relationships break

CPD
5, 1133–1162, 2009

down. Consistent with these simulations are observational evidence at Summit, Greenland that shows little to no changes in $\delta^{18}O_{prec}$ over the course of the Holocene (Alley et al., 1997). At Summit, the model simulates no change in $\delta^{18}O_{prec}$, but 1.5°C cooler temperatures in the early Holocene (Fig. 5). This simulated cooling is consistent with other proxy evidence from the coast of Greenland that suggests cooler temperatures in the Early Holocene (Kelly et al., 2008).

ITCZ related shifts of precipitation over oceans yields negative northern and positive southern $\delta^{18}O_{prec}$ anomalies in the tropics. Modeled changes in $\delta^{18}O_{prec}$ of southern Eurasia closely resemble changes inferred from Asian speleothem $\delta^{18}O$ records at millennial timescales (Fig. 6). The modeled tropical $\delta^{18}O_{prec}$ changes do not, however, follow precipitation changes; notably, from West Africa through Northeast Asia, $\delta^{18}O_{prec}$ is depleted, despite small and opposite sign precipitation changes (Fig. 2). Nor are the $\delta^{18}O_{prec}$ anomalies simply scaled to the magnitude of the local precipitation changes.

Closer examination of the simulated changes over China show no correlation between local precipitation and $\delta^{18}O_{prec}$ over these timescales; however, there is a strong correlation between $\delta^{18}O_{prec}$ and water vapor transport onto China from the Pacific (Fig. 7). In India, $\delta^{18}O_{prec}$ changes are associated with not only water vapor transport changes onto land, but also precipitation changes (Fig. 7). This relationship suggests that millennial $\delta^{18}O_{prec}$ changes inferred from tropical interior Asian $\delta^{18}O$ records from speleothems are recording alterations in water vapor export out of the tropics, and not local changes in precipitation as might be inferred from present day analogs (Schmidt and LeGrande, 2009). In coastal regions, observed (GNIP/IAEA) tropical Asian $\delta^{18}O$ records do correlate with local rainfall changes, but these changes are also highly correlated with the landward transport of water vapor from the oceans (Rozanski et al., 1993). Intensification of landward water vapor transport in the past simulations compared to modern is likely related to the enhanced boreal seasonality induced by orbital changes.

Associated with this shift in water export to the land are changes in the hydrological balance in related ocean regions. In the mid to early Holocene, simulated salinity and $\delta^{18}O_{sw}$ are lower in the Atlantic, particularly tropical to southern sub-tropical by ~0.5 psu and ~0.2‰. Indian Ocean salinities and $\delta^{18}O_{sw}$ decrease as well, by a slightly larger magnitude. Western tropical Pacific salinities and $\delta^{18}O_{sw}$ increase by up to ~0.6 psu and 0.3‰, respectively. The modern depletion (0.25‰ at the Mid-Holocene) of water isotopes in the Western Tropical Pacific matches well with paleosalinity reconstructions (Fig. 6 & Oppo et al., 2007). Rainfall over this area is generally enriched; $\delta^{18}O_{sw}$ and $\delta^{18}O_{precip}$ changes over oceans tend to be correlated.

The salinity (and $\delta^{18}O_{sw}$ contrast) between the Western Tropical Atlantic and the eastern Tropical Pacific was less in the early Holocene owing mainly to decreased water vapor transport across the isthmus of Panama. This modeled trend is at odds with some paleoclimate reconstructions (e.g., Schmidt et al., 2004). Perhaps this is due to a lack of sufficiently high resolution data for comparisons, or the model simulations could be incorrect owing to overly coarse topography over Panama, which might compromise the inter-basin transport simulation there.

3.3 Water vapor transport changes

The tropical hydrologic cycle is closed to first order; i.e., the vast majority of water evaporated, precipitates back in the tropics (Hoffmann, 2003). In all of our simulations, tropical water vapor is largely recycled, as indicated by the two near surface equator ward cells (Fig. 8b). Water vapor that does escape the tropics does so in the mid troposphere (~800 mb). The isotopic composition of water vapor exiting the tropics is −15‰ to −20‰ both in these simulations and in observations (Craig and Gordon, 1965; Lee et al., 2009). The modeled average isotopic composition of this end member changes very little over the course of the Holocene. There is a small (volume) complication for stratospheric water vapor, owing to alterations in atmospheric methane concentration (a source of depleted $\delta^{18}O$).

CPD
5, 1133–1162, 2009

The simulated flux of water vapor, however, changes dramatically over the course of the Holocene (Fig. 8c), with the export of water vapor out of the tropics over the oceans decreasing over the Western Pacific by ∼12% in the Mid-Holocene. Over land, enhanced boreal seasonality causes an increase in land-sea temperature contrasts, and tropical water vapor transport onto land was thus greater during the mid-Holocene than today. Within the tropics, there is a northward migration of the ITCZ of ∼10–15°. This paired with a northward shift of the ITCZ enhances water vapor transport onto West Africa. In Asia, this transport onto land was in general increased in the Mid-Holocene; e.g., flux onto China increases by 20%, onto West India increases by 29%; East Indian transport increases by 20% (Fig. 7).

Changes in northward water vapor transport (Fig. 8) imply changes in northward latent heat flux. Total atmospheric heat flux is a combination of this field and transport of dry static energy, and in these simulations, the magnitudes of changes in the two are similar (though regionally varying). Because of this fundamental link between atmospheric heat transport and water vapor flux, changes in $\delta^{18}O_{precip}$ for the Holocene might also be thought of as an indicator of changes in atmospheric heat transport, with a greater export of tropical latent heat associated with a greater export of depleted (−15 to −20‰) tropical water vapor.

3.4 Ocean circulation changes

Exchange (surface through mixed layer depth) between the Labrador Sea and the North Atlantic was diminished by 1/3 in the mid-Holocene. In the early Holocene, the remaining fluxes out of the Labrador Sea into the North Atlantic were fresher and depleted by 2‰ on average, and the mixed layer in the Northwestern Atlantic was much shallower.

Transport of saltier surface waters from the Indian Ocean (0.33‰ $\delta^{18}O_{sw}$) into the Atlantic was diminished by 25%, while transport of tropical Pacific waters into the Indian Ocean was decreased by 13% in the early Holocene compared to the pre-Industrial. Advection from the Eastern to the Western Tropical Pacific increased by 5%, with the

$\delta^{18}O_{sw}$ enriched by 0.1‰.

Overall, the alterations in ocean circulation worked to salinify the Pacific Ocean, and freshen the Atlantic (Fig. 4). The tropical western Pacific is 0.27 psu saltier and 0.1‰ enriched in $\delta^{18}O_{sw}$. The tropical eastern Pacific has smaller changes of a similar sign, while the Atlantic is 0.16 psu fresher and 0.1‰ depleted in $\delta^{18}O_{sw}$.

These changes lead to enhanced intermediate water formation in the North Pacific, which yields a positive feedback to Northern Hemisphere warming (created by the enhanced boreal insolation), and a means for regionally warmer temperatures in the North Pacific region that persisted through boreal winter.

In the pre-Industrial (control) simulation, there is a northward flux through the Bering Strait, though the simulated flux is significantly less than observed. In all of the other Holocene simulations, this flux reverses direction; by the early Holocene, this reversed flux has grown to 3 times the magnitude of that in the PI, and serves as a means to export freshwater out of the North Atlantic Ocean (via the Arctic). This reversal is driven by sea ice changes that are related to decreases in sea level pressure of ~2 mb and to a lesser extent by the surface freshwater balance (P-E+R) increasing by 8%. A 9 kya sensitivity study where the Bering Strait was closed resulted in a shutdown of NADW since the additional freshwater fluxes from the melting of the LIS "pooled" in the North Atlantic. (N.B., the Bering Strait likely opened several thousand years prior to the 9 kya simulation.) This result is suggestive of a means for the termination of the Younger Dryas, but follow-up work is required to quantify its likelihood. Surface and intermediate depth densities were greater in the Arctic, with the contrast of surface to deep water densities slightly reduced.

4 Isotope record comparisons

Seawater oxygen isotopes in the modern simulation compares favorably with observations (LeGrande and Schmidt, 2006), though the model tends to smooth zonal asymmetries. Further, the model does not attain the maximum depletion in Vostok Summit

as observed (Schmidt et al., 2005); this may be related to model difficulties in simulating steep topography and temperatures there. Atmospheric water vapor at the emission level in the atmosphere is similar to that observed, though the seasonal cycle differs in sign (J. Lee, personal communication).

The ModelE Holocene simulations can be quantitatively compared to relevant $\delta^{18}O$ records. Broad trends of increased $\delta^{18}O_{pr}$ from the early to late Holocene from Asian speleothem records is well reproduced (Fleitmann et al., 2003; Hu et al., 2008; Wang et al., 2005). Further, 0.2‰ to 0.3‰ mid-Holocene increases in Western Tropical Pacific $\delta^{18}O_{sw}$ are also simulated well in the model (Fig. 6; Stott et al., 2004). All Holocene simulations have $\delta^{18}O_{pr}$ at Summit, Greenland of −34.7‰ to −35‰ very similar to the observed range over the Holocene (Andersen et al., 2004). Simulated early Holocene oxygen isotopes are similar to observed in ice cores and marine sediment cores (Carlson et al., 2008). Simulated western tropical Pacific seawater oxygen isotopes are similar to those observed there, as well (Oppo et al., 2007).

Change in simulated salinity are significantly less than the ∼1 psu that would be predicted by the modern regional $\delta^{18}O_{sw}$ to salinity relationship (e.g., in LeGrande and Schmidt, 2006) in tropical western Atlantic, Caribbean, and Western Tropical Pacific. In some Gulf of Mexico locations, the change in $\delta^{18}O_{sw}$ would imply a roughly 3X magnitude change in salinity if the modern regional relationship between the two were applied (LeGrande and Schmidt, 2006). More work is required to understand means to quantitatively interpret $\delta^{18}O_{sw}$ signals as paleosalinity.

5 Discussion

Many of the existing sensitivity studies using ModelE-R have focused on sensitivity of the model to future projected greenhouse gas changes (e.g., Hansen et al., 2005). These results show that in a warmer (greenhouse driven) world, atmospheric circulation changes such that northward latent heat transport decreases and sensible heat increases – trends that follow from the changes in temperature and water mass in the

atmosphere. In our Mid- and Early Holocene simulations, the global temperature is slightly lower (owing to greenhouse gas changes), but Northern Hemisphere temperatures are increased (as a result of orbital changes). Water vapor content does indeed increase in the Northern Hemisphere, and decrease in the Southern Hemisphere (owing to slightly lower insolation and reduced greenhouse gases). The zonal mean changes in heat transport show a decrease in latent heat transport in the northern mid latitudes. These changes demonstrate a very complicated picture where enhanced seasonality drives large changes in land-sea temperature contrast, and this change dominates changes to water vapor and latent heat transport. This feature demonstrates the potential of determining model sensitivity to different "types" of climate change by simulating paleoclimate.

Water isotope fields show distinctive "fingerprints" of climate changes through the Holocene. In the atmosphere, these changes are very similar to latent heat changes. Latent heat transport changes dominate the total atmospheric heat transport changes, and explain the fundamental link between water vapor, temperature, and $\delta^{18}O$, even in continental tropical settings. The correlation between $\delta^{18}O_{pr}$ and precipitation in these locations breaks down since advective changes dominate the final $\delta^{18}O_{pr}$ signal. Terrestrial $\delta^{18}O$ changes in water isotopes represent alterations to the water vapor flux onto land. Thus, changes in temperature and $\delta^{18}O_{pr}$ at high latitudes are related, but the patterns of change in the two are not always identical. This feature leads to situations such as in the early Holocene where changes in temperature at Summit, Greenland are not captured in the $\delta^{18}O_{pr}$ signal.

Large changes in atmospheric water vapor transport have important consequences for seawater isotopes as well. Alterations in inter-basin exchange, land-sea amounts of precipitation, and tropical export of water vapor all have impacts on marine $\delta^{18}O$ records in addition to their terrestrial counterparts. Past reconstructions of $\delta^{18}O_{sw}$ thus can provide insight into atmospheric processes. The consequence, however, of this atmospheric connection is that simple links to other freshwater tracers is complicated. For instance, modern $\delta^{18}O_{sw}$ to salinity calibrations to determine past salinity given a

CPD
5, 1133–1162, 2009

$\delta^{18}O_{sw}$ record do not currently include estimates of variability due to atmospheric circulation changes. This study supports using modern $\delta^{18}O_{sw}$ to salinity relationships is a qualitative calibration, and it may be improved by expanding the terms (that $\delta^{18}O_{sw}$ depends on) to include more of the hydrologic cycle. These large changes in water vapor transport imply large changes in the salinity and $\delta^{18}O_{sw}$ end members, suggesting a means for improved interpretations of $\delta^{18}O_{sw}$. The pairing of oxygen isotope records with other proxy records for salinity may reduce uncertainty in salinity reconstructions as well as provide more insight into changes of the hydrologic cycle in general (Rohling, 2007).

We used eight time slices across the Holocene in order to provide greater confidence in $\delta^{18}O$ to climate inversions (8 data points). However, the majority of the features present in the mid-Holocene case are well represented in the 1 kya through 5 kya cases, with primarily the magnitude of anomalies changing. The Early Holocene case has the added complication of changes in ice sheets, and its patterns of climate change differ from those in the 6 kya case. From this result, it seems that transient, or high temporal resolution time slice through periods of ice sheet change are necessary, while transient/high temporal resolution time slice simulations of interstadials are less useful.

6 Conclusions

Forward modeling of the proxy climate tracers is essential in understanding the variability in the proxy climate archives. Oxygen isotopes record changes in the hydrologic cycle, meaning that complexities including temperature, precipitation, initial source composition, pathways to deposition, and mixing along the route always play a role in determining the final composition. The Holocene simulations suggest that during periods of large glaciations and large changes in glaciations, forward modeling may be very helpful in determining the temperature signal in the Greenland ice core $\delta^{18}O_{prec}$ records, for

CPD
5, 1133–1162, 2009

example. Models have an important role in elucidating which components of change in the hydrologic cycle are most responsible for variability at different timescales, and thus they provide a means for improved interpretations of proxy climate archives. The GISS model does capture the major features of Northern Hemisphere warming during the mid-Holocene. In the Early Holocene, Northern Hemisphere climate is consistent with the known rates of retreat of the North American ice sheets (Carlson et al., 2008). This match suggests that the model has appropriately sized responses to orbital changes and to small greenhouse gas changes. Caveats are that increases in Sahel rainfall and sea ice reductions from the mid to early Holocene are too small. In all, the GISS model reasonably simulates climate over the Holocene (compared to the proxy records), and the variability in these tracers provides a way to assess the skill of the model.

References

Alley, R. B., Mayewski, P. A., Sowers, T., Stuiver, M., Taylor, K. C., and Clark, P. U.: Holocene climatic instability: A prominent, widespread event 8200 yr ago, Geology, 25(6), 483–486, 1997.

Andersen, K. K., Azuma, N., Barnola, J. M., Bigler, M., Biscaye, P., Caillon, N., Chappellaz, J., Clausen, H. B., DahlJensen, D., Fischer, H., Fluckiger, J., Fritzsche, D., Fujii, Y., Goto-Azuma, K., Gronvold, K., Gundestrup, N. S., Hansson, M., Huber, C., Hvidberg, C. S., Johnsen, S. J., Jonsell, U., Jouzel, J., Kipfstuhl, S., Landais, A., Leuenberger, M., Lorrain, R., Masson-Delmotte, V., Miller, H., Motoyama, H., Narita, H., Popp, T., Rasmussen, S. O., Raynaud, D., Rothlisberger, R., Ruth, U., Samyn, D., Schwander, J., Shoji, H., Siggard-Andersen, M. L., Steffensen, J. P., Stocker, T., Sveinbjornsdottir, A. E., Svensson, A., Takata, M., Tison, J. L., Thorsteinsson, T., Watanabe, O., Wilhelms, F., White, J. W. C., and N. G. I. C. Project: High-resolution record of Northern Hemisphere climate extending into the last interglacial period, Nature, 431(7005), 147–151, 2004.

Berger, A. and Loutre, M. F.: Insolation Values for the Climate of the Last 10 000 000 Years, Quaternary Sci. Rev., 10(4), 297–317, 1991.

Brook, E. J., Harder, S., Severinghaus, J., Steig, E. J., and Sucher, C. M.: On the origin

and timing of rapid changes in atmospheric methane during the last glacial period, Global Biogeochem. Cy., 14(2), 559–572, 2000.
Carlson, A. E., Clark, P. U., Raisbeck, G. M., and Brook, E. J.: Rapid Holocene deglaciation of the Labrador sector of the Laurentide Ice Sheet, J. Climate, 20(20), 5126–5133, 2007.
Carlson, A. E., LeGrande, A. N., Oppo, D. W., Came, R. E., Schmidt, G. A., Anslow, F. S., Licciardi, J. M., and Obbink, E. A.: Rapid early Holocene deglaciation of the Laurentide ice sheet, Nature Geoscience, 1(9), 620–624, 2008.
Charles, C. D., Rind, D., Jouzel, J., Koster, R. D., and Fairbanks, R. G.: Seasonal Precipitation Timing and Ice Core Records, Science, 269(5221), 247–248, 1995.
Craig, H. and Gordon, L. I.: Deuterium and Oxygen 18 Variations in the Ocean and the Marine Atmosphere, Pisa, Italy, 1965.
Cuffey, K. M., Clow, G. D., Alley, R. B., Stuiver, M., Waddington, E. D., and Saltus, R. W.: Large Arctic Temperature-Change at the Wisconsin-Holocene Glacial Transition, Science, 270(5235), 455–458, 1995.
Dansgaard, W.: Stable isotopes in precipitation, Tellus, 16, 436–468, 1964.
Epstein, S., Buchsbaum, R., Lowenstam, A., and Urey, H. C.: Revised carbonate-water isotopic temperature scale, Geol. Soc. Am. Bull., 64, 1315–1325, 1953.
Fairbanks, R. G.: A 17 000-year glacio-eustatic sea level record: influence of glacial melting rates on the Younger Dryas event and deep-ocean circulation, Nature, 342, 637–642, 1989.
Fleitmann, D., Burns, S. J., Mudelsee, M., Neff, U., Kramers, J., Mangini, A., and Matter, A.: Holocene forcing of the Indian monsoon recorded in a stalagmite from Southern Oman, Science, 300(5626), 1737–1739, 2003.
Hansen, J., Nazarenko, L., Ruedy, R., Sato, M., Willis, J., Del Genio, A., Koch, D., Lacis, A., Lo, K., Menon, S., Novakov, T., Perlwitz, J., Russell, G., Schmidt, G. A., and Tausnev, N.: Earth's energy imbalance: Confirmation and implications, Science, 308(5727), 1431–1435, 2005.
Hansen, J., Sato, M., Ruedy, R., Kharecha, P., Lacis, A., Miller, R., Nazarenko, L., Lo, K., Schmidt, G. A., Russell, G., Aleinov, I., Bauer, S., Baum, E., Cairns, B., Canuto, V., Chandler, M., Cheng, Y., Cohen, A., Del Genio, A., Faluvegi, G., Fleming, E., Friend, A., Hall, T., Jackman, C., Jonas, J., Kelley, M.,Kiang, N. Y., Koch, D., Labow, G., Lerner, J., Menon, S., Novakov, T., Oinas, V., Perlwitz, J., Perlwitz, J., Rind, D., Romanou, A., Schmunk, R., Shindell, D., Stone, P., Sun, S., Streets, D., Tausnev, N., Thresher, D., Unger, N., Yao, M., and Zhang, S.: Climate simulations for 1880–2003 with GISS modelE, Clim. Dynam., 29(7–8), 661–696, 2007.

Haug, G. H., Hughen, K. A., Sigman, D. M., Peterson, L. C., and Röhl, U.: Southward migration of the intertropical convergence zone through the Holocene, Science, 293(5533), 1304–1308, 2001.
Hillaire-Marcel, C., de Vernal, A., Bilodeau, G., and Weaver, A. J.: Absence of deep-water formation in the Labrador Sea during the last interglacial period, Nature, 410(6832), 1073–1077, 2001.
Hoffmann, G.: Taking the pulse of the tropical water cycle, Science, 301(5634), 776–777, 2003.
Hu, C., Henderson, G. A., Huang, J., Xie, S., Sun, Y., and Johnson, R. G.: Quantification of Holocene Asian monsoon rainfall from spatially separated cave records, Earth Planet. Sc. Lett., 226(3–4), 221–232, 2008.
Indermuhle, A., Stocker, T. F., Joos, F., Fischer, H., Smith, H. J., Wahlen, M., Deck, B., Mastroianni, D., Tschumi, J., Blunier, T., Meyer, R., and Stauffer, B.: Holocene carbon-cycle dynamics based on CO_2 trapped in ice at Taylor Dome, Antarctica, Nature, 398(6723), 121–126, 1999.
Jouzel, J., Vimeux, F., Caillon, N., Delaygue, G., Hoffmann, G., Masson-Delmotte, V., and Parrenin, F.: Magnitude of isotope/temperature scaling for interpretation of central Antarctic ice cores, J. Geophys. Res.-Atmos., 108(D12), 4361, doi:10.1029/2002JD002677, 2003.
Kelly, M. A., Lowell, T. V., Hall, B. L., Schaefer, J. M., Finkel, R. C., Goehring, B. M., Alley, R. B., and Denton, G. H.: A Be-10 chronology of lateglacial and Holocene mountain glaciation in the Scoresby Sund region, east Greenland: implications for seasonality during lateglacial time, Quaternary Sci. Rev., 27(25–26), 2273–2282, 2008.
Lee, J., Noone, D., LeGrande, A. N., and Bowman, K.: Comparisons between Tropospheric Emission Spectrometer (TES) observations and isotope enabled GCMs, J. Geophys. Res. Atmos., in preparation, 2009.
LeGrande, A. N. and Schmidt, G. A.: Global gridded dataset of the oxygen isotopic composition in seawater, Geophys. Res. Lett., 33(12), L12604, doi:10.1029/2006GL026011, 2006.
Licciardi, J. M., Clark, P. U., Jenson, J. W., and Macayeal, D. R.: Deglaciation of a soft-bedded Laurentide Ice Sheet, Quaternary Sci. Rev., 17(4–5), 427–448, 1998.
Maher, B. A.: Holocene variability of the East Asian summer monsoon from Chinese cave records: a re-assessment, Holocene, 18(6), 861–866, 2008.
Masson-Delmotte, V., Kageyama, M., Braconnot, P., Charbit, S., Krinner, G., Ritz, C., Guilyardi, E., Jouzel, J., Abe-Ouchi, A., Crucifix, M., Gladstone, R. M., Hewitt, C. D., Kitoh, A., LeGrande, A. N., Marti, O., Merkel, U., Motoi, T., Ohgaito, R., Otto-Bliesner, B., Peltier, W. R.,

Ross, I., Valdes, P. J., Vettoretti, G., Weber, S. L., Wolk, F., and Yu, Y.: Past and future polar amplification of climate change: climate model intercomparisons and ice-core constraints, Clim. Dynam., 26(5), 513–529, 2006.

McManus, J. F., Francois, R., Gherardi, J. M., Keigwin, L. D., and Brown-Leger, S.: Collapse and rapid resumption of Atlantic meridional circulation linked to deglacial climate changes, Nature, 428(6985), 834–837, 2004.

Oppo, D. W., Schmidt, G. A., and LeGrande, A. N.: Seawater isotope constraints on tropical hydrology during the Holocene, Geophys. Res. Lett., 34, L13701, doi:10.1029/2007GL030017, 2007.

Pearman, P. B., Randin, C. F., Broennimann, O., Vittoz, P., van der Knaap, W. O., Engler, R., Le Lay, G., Zimmermann, N. E., and Guisan, A.: Prediction of plant species distributions across six millennia, Ecol. Lett., 11(4), 357–369, 2008.

Roden, J. S., Lin, G. G., and Ehleringer, J. R.: A mechanistic model for interpretation of hydrogen and oxygen isotope ratios in tree-ring cellulose, Geochim. Cosmochim. Ac., 64(1), 21–35, 2000.

Rohling, E. J.: Progress in paleosalinity: Overview and presentation of a new approach, Paleoceanography, 22(3), 2007.

Rozanski, K., Araguas-Araguas, L., and Gonfiantini, R.: Isotopic patterns in modern global precipitation, 78, American Geophysical Union, Washington, D.C., 1993.

Schmidt, G. A.: Error analysis of paleosalinity calculations, Paleoceanography, 14(3), 422–429, 1999.

Schmidt, G. A., Hoffmann, G., Shindell, D. T., and Hu, Y. Y.: Modeling atmospheric stable water isotopes and the potential for constraining cloud processes and stratosphere-troposphere water exchange, J. Geophys. Res.-Atmos., 110(D21), D21314, doi:10.1029/2005JD005790, 2005.

Schmidt, G. A. and LeGrande, A. N.: Controls on Speleothem isotope variability, in preparation, 2009.

Schmidt, G. A., LeGrande A. N., and Hoffmann, G.: Water isotope expressions of intrinsic and forced variability in a coupled ocean-atmosphere model, J. Geophys. Res.-Atmos., 112, D10103, doi:10.1029/2006JD007781, 2007.

Schmidt, G. A., Reudy, R., Hansen, J. E., Aleinov, I., Bell, N., Bauer, M., Bauer, S., Cairns, B., Canuto, V., Cheng, Y., Del Genio, A., Faluvegi, G., Friend, A. D., Hall, T. M., Hu, Y., Kelley, M., Kiang, N. Y., Koch, D., Lacis, A. A., Lerner, J., Lo, K. K., Miller, R. L., Nazarenko,

L., Oinas, V., Perlwitz, J., Perlwitz, J., Rind, D., Romanou, A., Russell, G. L., Sato, M., Shindell, D. T., Stone, P. H., Sun, S., Tausnev, N., Thresher, D., and Yao, M.-Y.: Present day atmospheric simulations using GISS ModelE: Comparison to in-situ, satellite and reanalysis data, J. Climate, 19, 153–192, 2006.

Schmidt, M. W., Spero, H. J., and Lea, D. W.: Links between salinity variation in the Caribbean and North Atlantic thermohaline circulation, Nature, 428(6979), 160–163, 2004.

Sowers, T., Alley, R. B., and Jubenville, J.: Ice core records of atmospheric N_2O covering the last 106 000 years, Science, 301(5635), 945–948, 2003.

Stott, L., Cannariato, K., Thunell, R., Haug, G. H., Koutavas, A., and Lund, S.: Decline of surface temperature and salinity in the western tropical Pacific Ocean in the Holocene epoch, Nature, 431(7004), 56–59, 2004.

Stroeve, J., Holland, M. M., Meier, W., Scambos, T., and Serreze, M.: Arctic sea ice decline: Faster than forecast, Geophys. Res. Lett., 34(9), doi:10.1029/2007GL029703, 2007.

Wang, Y. J., Cheng, H., Edwards, R. L., An, Z. S., Wu, J. Y., Shen, C. C., and Dorale, J. A.: A high-resolution absolute-dated Late Pleistocene monsoon record from Hulu Cave, China, Science, 294(5550), 2345–2348, 2001.

Wang, Y. J., Cheng, H., Edwards, R. L., He, Y. Q., Kong, X. G., An, Z. S., Wu, J. Y., Kelly, M. J., Dykoski, C. A., and Li, X. D.: The Holocene Asian monsoon: Links to solar changes and North Atlantic climate, Science, 308(5723), 854–857, 2005.

Wanner, H., Beer, J., Butikofer, J., Crowley, T. J., Cubasch, U., Fluckiger, J., Goosse, H., Grosjean, M., Joos, F., Kaplan, J. O., Kuttel, M., Muller, S. A., Prentice, I. C., Solomina, O., Stocker, T. F., Tarasov, P., Wagner, M., and Widmann, M.: Mid- to Late Holocene climate change: an overview, Quaternary Sci. Rev., 27(19–20), 1791–1828, 2008.

Werner, M., Mikolajewicz, U., Heimann, M., and Hoffmann, G.: Borehole versus isotope temperatures on Greenland: Seasonality does matter, Geophys. Res. Lett., 27(5), 723–726, 2000.

Table 1. Changes in boundary conditions for Holocene simulations include changes to greenhouse gases (Indermuhle et al., 1999) and perihelion in Julian days (Berger and Loutre, 1991) for all simulations. The 9 kya simulation includes the Laurentide Ice Sheet (Licciardi et al., 1998), and the correspondent adjustment to mean ocean salinity to 35 psu and $\delta^{18}O_{sw}$ to +0.33 ‰ (Fairbanks, 1989).

Time (kya)	CO_2 (fraction)	CH_4 (fraction)	N_2O (fraction)	Perihelion	Ice
0	1	1	1	2.70	No
1	0.98	0.87	0.94	349.6	No
2	0.98	0.81	1.00	332.3	No
3	0.97	0.80	0.95	314.9	No
4	0.96	0.77	0.94	297.4	No
5	0.95	0.71	0.94	279.9	No
6	0.95	0.71	0.82	262.4	No
9	0.93	0.83	0.89	210.4	Yes*

CPD
5, 1133–1162, 2009

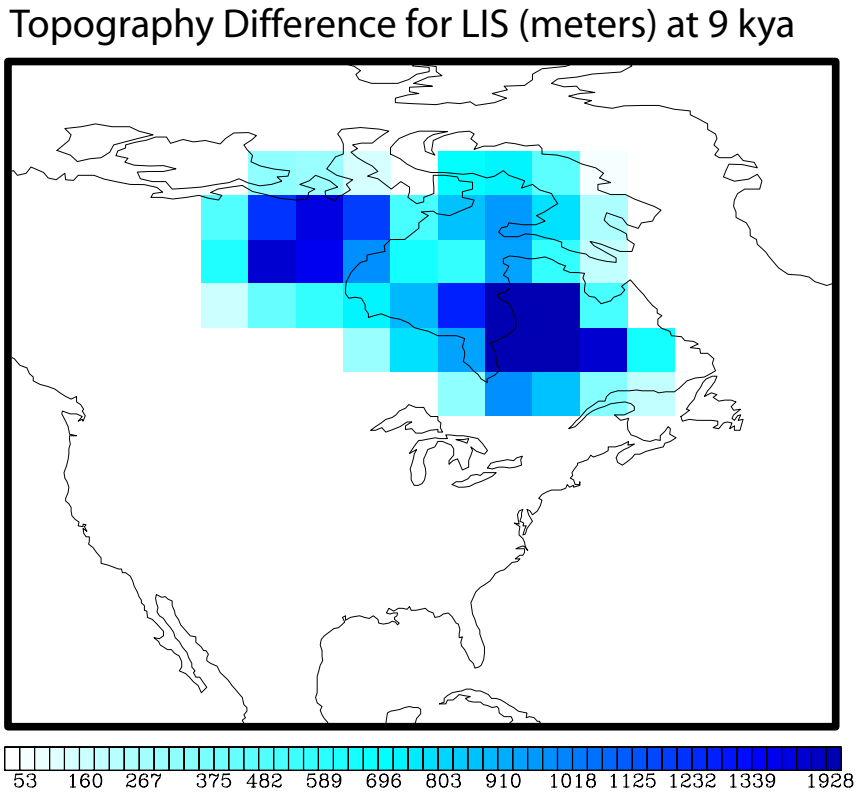

Fig. 1. Topography anomaly at 9 kya showing the remnant Laurentide Ice Sheet. Adapted from Licciardi et al. (1998).

CPD
5, 1133–1162, 2009

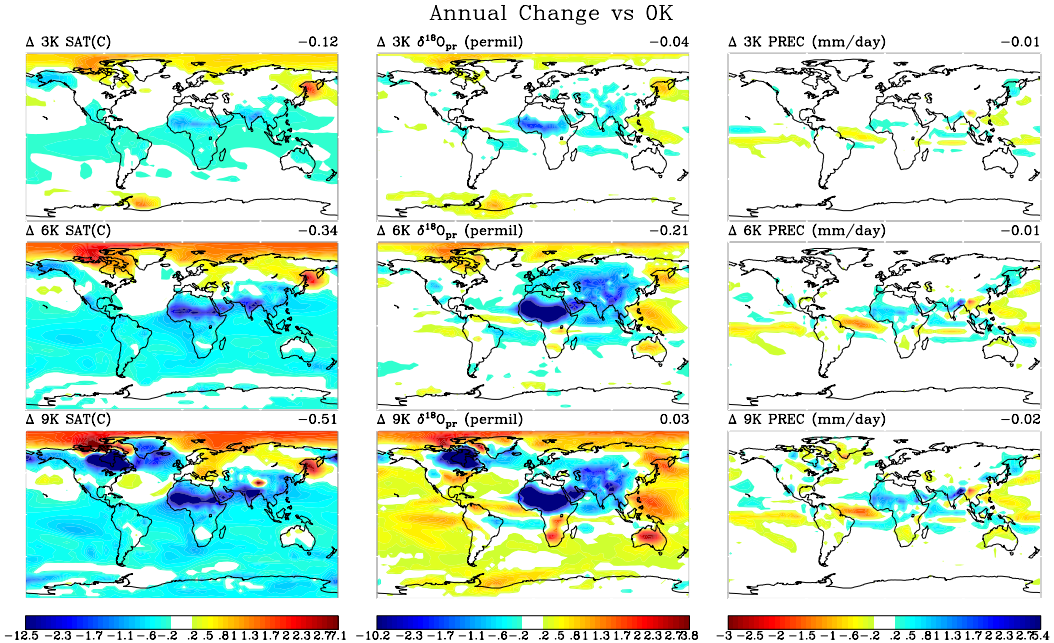

Fig. 2. Anomaly atmosphere climatology at 3 kyr (top), 6 kyr (middle), and 9 kyr (bottom) for SAT (left), δ^{18}Opr (middle), and precipitation (right). Values reported are greater than 99% significance (student's t-test) given the decadal variability about the 100-year mean.

CPD
5, 1133–1162, 2009

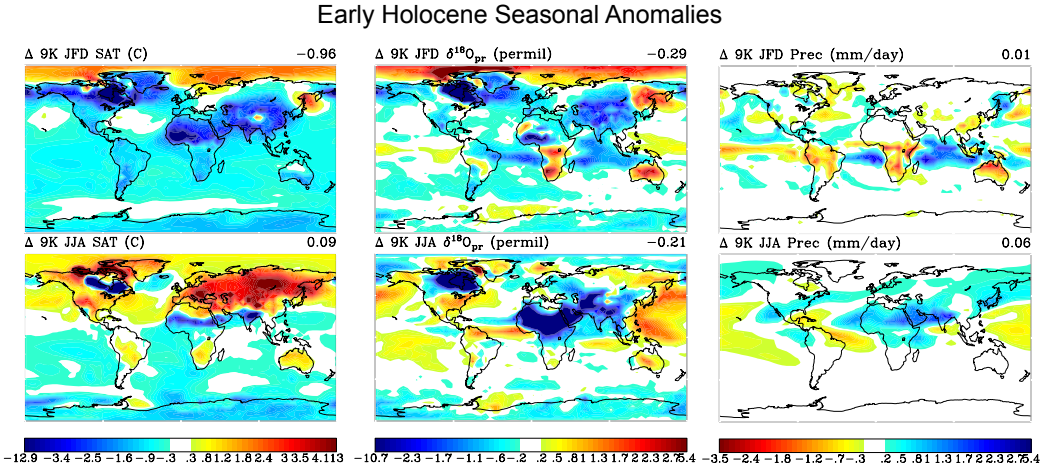

Fig. 3. Seasonal atmospheric changes at 9 kyr boreal winter (bottom) and boreal summer (top) for SAT (left), δ^{18}Opr (middle), and precipitation (right).

CPD
5, 1133–1162, 2009

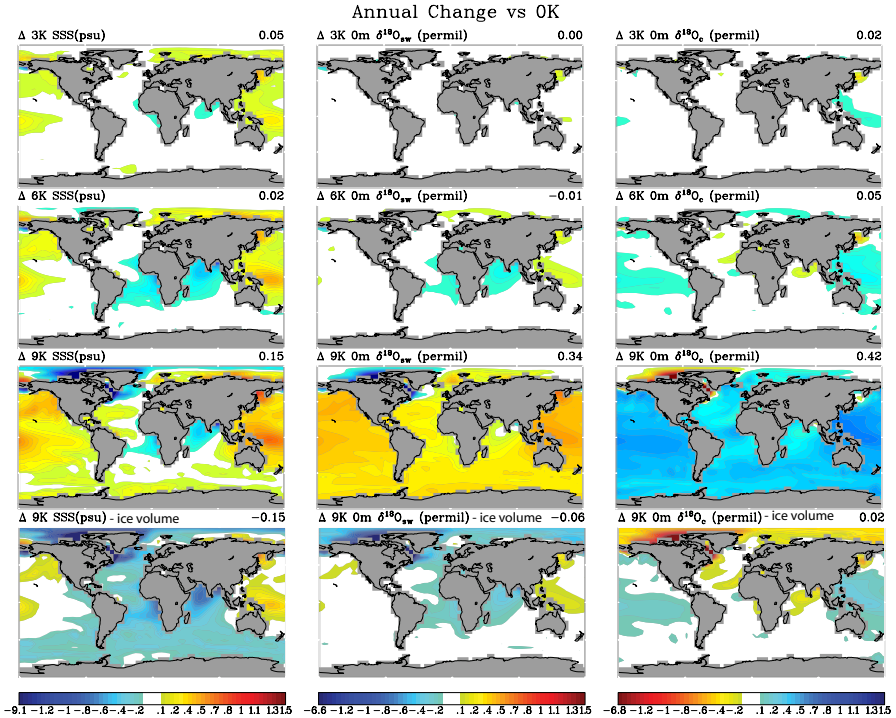

Fig. 4. Anomaly ocean climatology at 3 kyr (top), 6 kyr (upper middle), 9 kyr (lower middle), and 9 kyr less ice volume effects (bottom) for SSS (left), surface δ^{18}Osw (middle), and surface δ^{18}Ocalcite (right). Values reported are greater than 99% significance (student's t-test) given the decadal variability about the 100-year mean.

CPD
5, 1133–1162, 2009

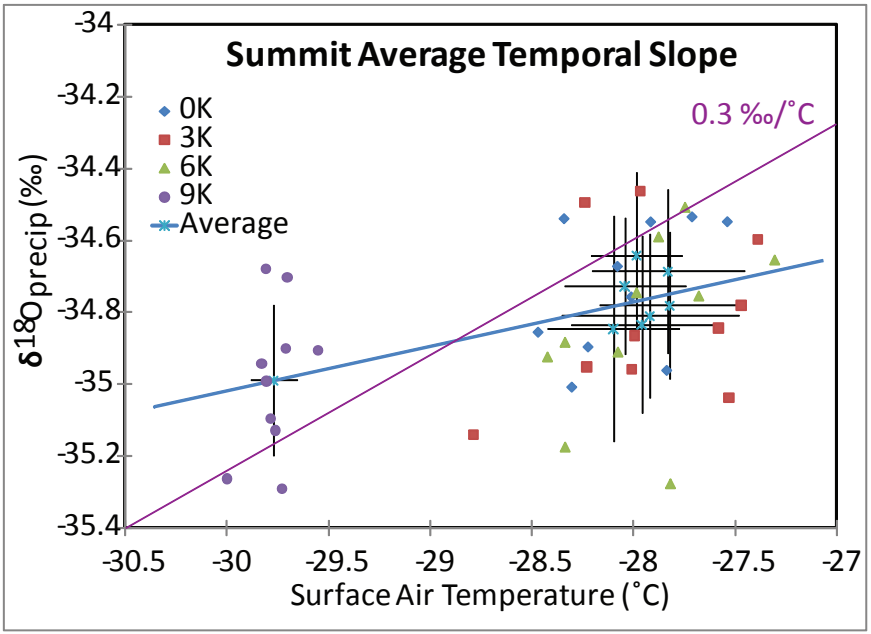

Fig. 5. Simulated annually averaged δ^{18}Opr from Summit, Greenland for all eight time slices (1σ variation in the decadal mean, black bars, about the century average, blue asterisk) are plotted against surface air temperature (˚C). The standard relationship between the two, 0.3‰/˚C (Cuffey et al., 1995) is plotted in purple, the simulated Early Holocene to modern trend is plotted in light blue.

CPD
5, 1133–1162, 2009

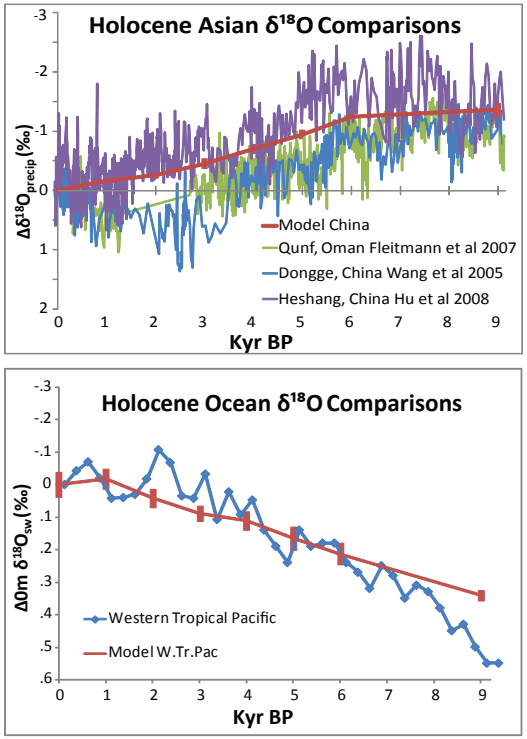

Fig. 6. (Upper) Annually averaged simulated δ^{18}Opr changes over China (44 grid points) with 1 σ variability for decadal average about the model 100-year mean compared to speleothem δ^{18}O from Oman (Fleitmann et al., 2007), Dongge, China (Wang et al., 2005), and Heshang, China (Hu et al., 2008). (Lower) Annually averaged simulated surface δ^{18}Osw changes with 1σ variability for decadal average about the model 100-year mean for the Western Tropical Pacific compared to measured (Stott et al., 2004). Values reported are normalized to modern. Ice volume changes have not been taken into account.

CPD
5, 1133–1162, 2009

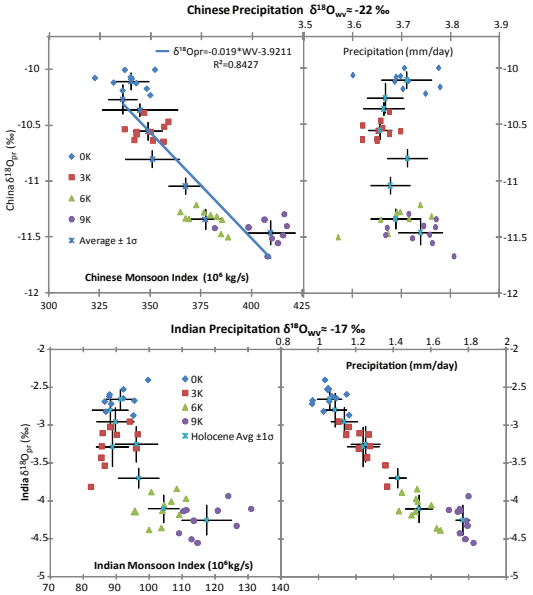

Fig. 7. Simulated annually averaged δ^{18}Opr from China (~30 grid boxes, above) and India (~12 grid boxes, below) for all eight time slices (1σ variation in the decadal mean, black bars, about the century average, blue asterisk) are plotted (left) against a monsoon index – onto land water vapor transport from the Indian or Pacific oceans – and (right) against precipitation (mm/day) averaged for the same region in China (above) and India (below). The monsoon index here is defined as the integrated JJA water vapor transport across the Chinese (above) and Indian (below) land-sea margin. Individual decadal averages appear for the 0 k (blue diamonds), 3 k (red squares), 6 k (green triangles), and 9 k (purple circles) cases. "Monsoon" and δ^{18}Opr are inversely related, with greater water vapor transport onto land associated with more depleted rainfall on land in both, while local Chinese precipitation and δ^{18}Opr are uncorrelated, and Indian precipitation and δ^{18}Opr are correlated.

CPD
5, 1133–1162, 2009

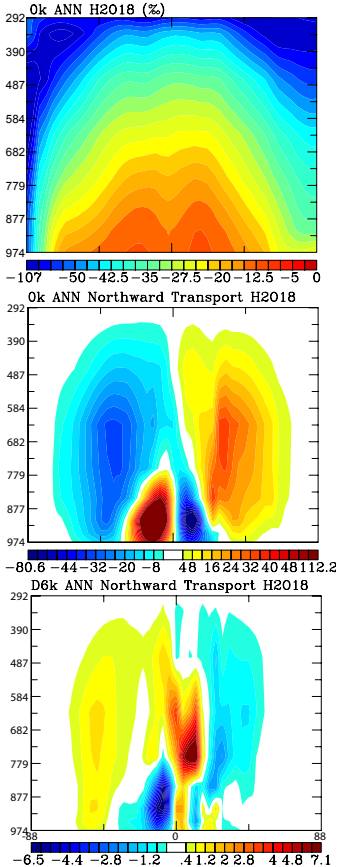

Fig. 8. Zonally averaged δ^{18}Opr (‰) in the preindustrial and the anomaly in the mid-Holocene. Zonally averaged northward ^{18}O (10^7 kg/s) transport in the preindustrial and the anomaly in the mid-Holocene.

CPD
5, 1133–1162, 2009